# Phase coexistence in a polydisperse charged hard-sphere fluid: Polymer mean spherical approximation

Yurij V. Kalyuzhnyi[a)]
*Institute for Condensed Matter Physics, Svientsitskoho 1, 79011 Lviv, Ukraine*

Gerhard Kahl
*Center for Computational Materials Science (CMS) and Institut für Theoretische Physik, TU Wien, Wiedner Hauptstraße 8-10, A-1040 Wien, Austria*

Peter T. Cummings
*Department of Chemical Engineering, Vanderbilt University, Nashville, Tennessee 37235-1604 and Chemical Sciences Division, Oak Ridge National Laboratory, Oak Ridge, Tennessee 27831-6110*

(Received 18 July 2005; accepted 1 August 2005; published online 23 September 2005)

We have reconsidered the phase behavior of a polydisperse mixture of charged hard spheres (CHSs) introducing the concept of minimal size neutral clusters. We thus take into account ionic association effects observed in charged systems close to the phase boundary where the properties of the system are dominated by the presence of neutral clusters while the amount of free ions or charged clusters is negligible. With this concept we clearly pass beyond the simple level of the mean spherical approximation (MSA) that we have presented in our recent study of a polydisperse mixture of CHS [Yu. V. Kalyuzhnyi, G. Kahl, and P. T. Cummings, J. Chem. Phys. **120**, 10133 (2004)]. Restricting ourselves to a 1:1 and possibly size-asymmetric model we treat the resulting polydisperse mixture of neutral, polar dimers within the framework of the polymer MSA, i.e., a concept that—similar as the MSA—readily can be generalized from the case of a mixture with a finite number of components to the polydisperse case: again, the model belongs to the class of truncatable free-energy models so that we can map the formally infinitely many coexistence equations onto a finite set of coupled, nonlinear equations in the generalized moments of the distribution function that characterizes the system. This allows us to determine the *full* phase diagram (in terms of binodals as well as cloud and shadow curves), we can study fractionation effects on the level of the distribution functions of the coexisting daughter phases, and we propose estimates on how the location of the critical point might vary in a polydisperse mixture with an increasing size asymmetry and polydispersity. © *2005 American Institute of Physics*.
[DOI: 10.1063/1.2042347]

## I. INTRODUCTION

Even though the restricted primitive model (RPM) represents a suitable model for electrolytes or molten salts (for an overview see Ref. 1), this is certainly not the case as we pass over to systems of charged *mesoscopic* particles, such as charged microgels, colloids, or micelles. The idealizing assumption of equally sized positively and negatively charged particles in the RPM (a property which we shall also call "bidisperse") is no longer justified in colloidal suspensions: here the particles are—as a consequence of the production process—rather polydisperse in their properties (such as size, interactions, etc.) and therefore a *polydisperse* mixture of charged hard spheres (CHSs) is undoubtedly a more appropriate model.

For a theoretician, however, a reliable description of a polydisperse system represents a formidable problem, since standard methods (as they exist for one- or two-component systems over a large range of sophistication[2]) are—at least at present—hardly available: computer simulations are disproportionately more expensive than for one-component systems—for a recent contribution see Ref. 3—which explains the lack of a considerable amount of reference data for polydisperse mixtures up to date; and theoretical concepts that allow to determine the *full* phase diagram (including an explicit determination of the distribution functions of the coexisting daughter phases) on a *quantitative* level are scarce and those few concepts that can be used are rather complex.[4] Despite these implications, there is definitely a need to obtain more information about such systems: academic interest will certainly focus on polydispersity as such, which leads to intriguing phase phenomena and fractionation effects;[4] and technology, on the other hand, will rather be interested in the properties of realistic polydisperse charged systems, such as the ones mentioned above.

In a recent study[5] we have made a first step to tackle this problem and have treated polydisperse mixtures of CHS within the framework of the mean spherical approximation (MSA). We have used the standard access to polydisperse systems, which are viewed as mixtures with an infinite number of components:[6] each species is characterized by a continuous index variable $\xi$ and the amount of particles in each

[a)]Electronic mail: yukal@icmp.lviv.ua

 

species $\xi$ is defined via the distribution function $\mathcal{I}(\xi)$, which is positive and normalized, i.e., $\int_0^\infty d\xi \mathcal{I}(\xi)=1$; $\mathcal{I}(\xi)d\xi$ is the fraction of particles with species index $\bar{\xi} \in [\xi, \xi+d\xi]$. Based on this picture we have used the expressions that are available in the literature for the thermodynamic and structural properties of a mixture of CHS (Refs. 7 and 8) with an arbitrary, but finite number of components; they can readily be generalized to the polydisperse case. It turns out that this access leads to a so-called truncatable free-energy model,[4] where the thermodynamic properties can be expressed by a finite (but still rather large) number of generalized moments of the distribution function $\mathcal{I}(\xi)$ that characterizes the system. Thus the formally infinitely many coexistence equations that determine phase equilibrium in a polydisperse mixture are mapped onto a finite set of coupled, highly nonlinear equations in these generalized moments which can be solved with suitable algorithms. Access to describe polydisperse mixtures via the truncatable free-energy model seems to be—at least at present—one of the rare viable routes towards a quantitative determination of the full phase diagram (in terms of binodals as well as cloud and shadow curves) of such systems.

However, our MSA approach[5] did not lead—as it might have been expected—to quantitatively correct results, since MSA is definitely inappropriate to calculate the phase diagram of charged systems. This failure of MSA can be traced back to subtle physical phenomena, which are characteristic for charged systems; these are revealed in careful analysis of computer simulation data[9–15] and can be confirmed in theoretical studies:[16–23] in the vicinity of the phase boundaries neutral ionic clusters of different size (i.e., dimers, trimers, …) are formed as a consequence of the strong Coulomb attraction while free ions or charged clusters play only a minor role. And MSA, being a linearized theory, is definitely inadequate to treat strongly interacting systems. This deficiency is reflected by the large discrepancies in the location of the critical point between MSA data and computer simulation results, which—at present—can be considered as exact reference data: for the bidisperse mixture (RPM) critical parameters obtained within MSA differ by a factor of $\sim 1.6$ in temperature and $\sim 0.2$ in density from the simulation data.

To make up for this deficiency we propose in the present contribution a more sophisticated concept that explicitly takes into account these association effects. To this end we have introduced the framework of minimal size neutral clusters (MSNCs), i.e., an idea that had turned out to be successful in studies both of the charge-symmetric and the size-asymmetric RPMs (see below). In this concept it is assumed that all the clusters formed in a charged system upon association are represented by the MSNC, i.e., by dimers in the 1:1 RPM, trimers in the 1:2 model, and $(m+1)$-mers in the $1:m$ model. In an effort to treat such a system of neutral, polar clusters, the polymer MSA (PMSA) was successfully utilized: PMSA (Refs. 19, 21, and 24–26) is a MSA version of the product-reactant Ornstein-Zernike approach,[27–30] which, in turn, originates from Wertheim's multidensity integral-equation theory for associating fluids.[31,32] A preliminary presentation of the formalism along with the first results has been presented in Ref. 33. In recent contributions PMSA was used to predict the liquid-gas phase diagram of 1:1 and 1:2 size-symmetric primitive models for electrolytes.[19,21] Although agreement between this theory and corresponding computer simulation was still not perfect, substantial improvement over the simple MSA predictions was achieved; the critical temperature differs now by a factor of 1.3 and the critical density by a factor of approximately 0.6, respectively. We also mention applications of this concepts for a $1:m$ highly size-asymmetric RPM.[20]

In an effort to treat the polydisperse mixture of neutral clusters within the PMSA, we have generalized the corresponding expressions for a mixture with a finite number of components to the polydisperse case. Again, the resulting expressions for the structural and thermodynamic properties depend only on a finite number of generalized moments of $\mathcal{I}(\xi)$, i.e., we deal again with a truncatable free-energy model. Based on this concept we have considered two-phase coexistence and have derived the corresponding coexistence equations for the unknown generalized moments of the coexisting daughter phases. We have determined the full phase diagram (in terms of binodals, as well as cloud and shadow curves) and the distribution functions of the daughter phases which allow us to study fractionation effects on a quantitative level. We have considered in detail the phase behavior of two polydisperse mixtures, one of them being size symmetric, the other one size asymmetric. The results are presented and discussed.

The paper is organized as follows: In Sec. II we present the model and discuss the consequences of the MSNC concept on the distribution function that characterizes the system. In Sec. III we present the PMSA formalism that helps us to describe the polydisperse mixture of the neutral, polar dimers; we derive expressions for the thermodynamic properties and present the set of equations that fix phase equilibrium. Section IV is dedicated to the discussion of our results: we start by specifying the systems and then present and discuss the results we have obtained for the phase diagrams and the distribution functions of the coexisting daughter phases. We finally present an estimate of how the location of the critical point might vary with size asymmetry and polydispersity and close the paper with concluding remarks.

## II. THE MODEL AND DISTRIBUTIONS

### A. The multicomponent model

We introduce our polydisperse model via its discrete, multicomponent representation and consider an $M$-component mixture of CHS immersed in a dielectric continuum with a dielectric constant $\epsilon$ at a temperature $T[\beta=(k_BT)^{-1}]$ and a number density $\rho$. Particles of species $i$ are characterized by a diameter $\sigma_i$ and a charge $ez_i$ ($e$ being the elementary charge), and a (partial) number density $\rho_i=N_i/V$, where $N_i$ is the number of the particles of species $i$ and $V$ is the volume of the system; therefore, $\rho=\Sigma_i\rho_i$ and we further introduce the concentrations, $x_i=\rho_i/\rho$ with $\Sigma_i x_i=1$. The pair potentials $\Phi_{ij}(r)$ acting between the particles of species $i$ and $j$ are given by

$$\Phi_{ij}(r) = \begin{cases} \infty, & 0 \leqslant r \leqslant \sigma_{ij} \\ e^2 z_i z_j / \epsilon r, & \sigma_{ij} < r \leqslant \infty, \end{cases} \tag{1}$$

where $\sigma_{ij} = (\sigma_i + \sigma_j)/2$. The system is neutral, thus the following relation is satisfied:

$$\sum_i x_i z_i = 0. \tag{2}$$

### B. The polydisperse model

To extend the discrete model presented above to the polydisperse case one has to make the transition from the discrete species index $i$ to a continuous index variable $\xi$, which is distributed according to a positive, normalized distribution function $\mathcal{I}(\xi)$. This function replaces the discrete set of concentrations $\{x_i\}$, and summations over the index $i$ now become integrations with respect to the continuous variable $\xi$. Since for the present model each species is defined by its size and charge, $\sigma$ and $z$, the most appropriate choice for $\xi$ is the set of the continuously distributed random variables, $\sigma$ and $z$, distributed according to the distribution function $\mathcal{I}(\sigma, z) \geqslant 0$, which satisfies the following normalizing condition:

$$\int_0^\infty d\sigma \int_{-\infty}^\infty dz \mathcal{I}(\sigma, z) = 1. \tag{3}$$

Further, the potentials of the discrete systems $\Phi_{ij}(r)$ are replaced by their respective counterparts in the polydisperse system $\Phi(r; \sigma_1, z_1, \sigma_2, z_2)$.

It is convenient to split the distribution function $\mathcal{I}(\sigma, z)$ into two contributions according to

$$\mathcal{I}(\sigma, z) = \alpha_+ \mathcal{I}_+(\sigma, z) + \alpha_- \mathcal{I}_-(\sigma, z), \tag{4}$$

where $\mathcal{I}_\pm(\sigma, z)$ describe the distribution and $\alpha_\pm$ quantify the fractions of positively and negatively charged particles, respectively. Thus

$$\begin{aligned} &\mathcal{I}_+(\sigma, z) = 0 \quad \text{for } z < 0, \\ &\mathcal{I}_-(\sigma, z) = 0 \quad \text{for } z \geqslant 0. \end{aligned} \tag{5}$$

Each of the functions $\mathcal{I}_\pm(\sigma, z)$ is normalized

$$\int_0^\infty d\sigma \int_{-\infty}^\infty dz \mathcal{I}_\pm(\sigma, z) = 1. \tag{6}$$

In the polydisperse case the charge neutrality condition (2) reads

$$\alpha_+ \langle z \rangle_+ + \alpha_- \langle z \rangle_- = 0, \tag{7}$$

where

$$\langle z \rangle_\pm = \int_0^\infty d\sigma \int_{-\infty}^\infty dz z \mathcal{I}_\pm(\sigma, z). \tag{8}$$

As it will become evident in a later context it is useful to relate our polydisperse CHS mixture to a binary (bidisperse) CHS mixture; to this end we define integers $m_+$ and $m_-$ via

$$\frac{\langle z \rangle_+}{\langle z \rangle_-} = -\frac{m_+}{m_-}, \tag{9}$$

where $m_+$ and $m_-$ are integer numbers with no multipliers in common. If we then consider the limit that the distribution functions $\mathcal{I}_\pm(\sigma, z)$ of the system become more and more pronounced with respect to $z$, until they become delta functions located at $\langle z \rangle_+$ and $\langle z \rangle_-$, respectively, then we end up with an $m_+ : m_-$ primitive model of an electrolyte. Thus, our polydisperse system can be seen as a polydisperse generalization of the corresponding primitive model for an electrolyte.

Further, relation (9) enables us to establish a connection between the polydisperse CHS fluid in question and a (polydisperse) fluid of MSNC. To this end we proceed as follows: we assume that all MSNCs are of the same size and that—similar to the case of a bidisperse CHS fluid[19,21]—they consist of $m_-$ positively charged particles with charge $z_+$ and of $m_+$ negatively charged particles with charge $z_-$, satisfying the "global" charge neutrality condition

$$z_- = -\frac{m_-}{m_+} z_+. \tag{10}$$

However, in the polydisperse case this condition is not sufficient to construct such MSNCs and one has to impose, in addition, "local" charge neutrality condition, which reads

$$z_+ dN_+(z_+) = -z_- dN_-(z_-), \tag{11}$$

with $dN_\pm(z_\pm) = \alpha_\pm F_\pm(z_\pm) |dz_\pm|$ and

$$F_\pm(z) = \int_0^\infty d\sigma \mathcal{I}_\pm(\sigma, z). \tag{12}$$

This additional charge neutrality condition guarantees that the total charge accumulated by particles with a charge "located" in the interval $dz_+$ around $z_+$ has the same absolute value as the total charge accumulated by particles with a charge in the interval $dz_-$ around $z_-$, where, in addition, $z_+$ and $z_-$ are related via (10).

From the above relations one can easily deduce

$$F_-(z) = \frac{m_+}{m_-} F_+\left(-\frac{m_+}{m_-} z\right). \tag{13}$$

Thus the concept of the MSNC approach extended to the polydisperse CHS fluid introduces a restriction on the distribution functions $F_+(z)$ and $F_-(z)$ which will have consequences on the results (see Sec. IV).

So far we have been considering the general case of the distribution function $\mathcal{I}(\sigma, z)$, which allows an independent variation of the charge and of the size of the particles. In what follows we will introduce a distribution function, which strongly correlates these two parameters, i.e.,

$$\mathcal{I}(\sigma, z) = f_\pm(\sigma) \delta\left(z - \langle z \rangle_\pm \frac{\sigma^2}{\langle \sigma^2 \rangle_\pm}\right), \tag{14}$$

where

$$\langle \sigma^2 \rangle_\pm = \int_0^\infty d\sigma \sigma^2 f_\pm(\sigma) \tag{15}$$

and the distribution functions $f_\pm(\sigma)$ are normalized

$$\int_0^\infty d\sigma f_\pm(\sigma) = 1. \tag{16}$$

The first reason for this particular choice for the distribution functions is the fact that the factorized ansatz (14) reduces the amount of numerical efforts required to solve the coexistence conditions (see below). In addition, this choice is also physically sound, since the functional form (14) implies that the charge of the particle $z_\pm$ is proportional to its surface,

$$z_\pm = \langle z \rangle_\pm \frac{\sigma_\pm^2}{\langle \sigma^2 \rangle_\pm}. \tag{17}$$

Again, the $f_\pm(\sigma)$ are not independent; to derive their relation, we first calculate the $F_\pm(\sigma)$ for this particular choice of $\mathcal{I}(\sigma,z)$—see Eq. (14)—and obtain

$$F_\pm(z) = f_\pm(\hat{\sigma}_\pm) \frac{\langle \sigma^2 \rangle_\pm}{2|\langle z \rangle_\pm|} \frac{1}{\hat{\sigma}_\pm}, \tag{18}$$

with

$$\hat{\sigma}_\pm = \sqrt{|z| \frac{\langle \sigma^2 \rangle_\pm}{|\langle z \rangle_\pm|}}. \tag{19}$$

Using then relation (13), which is valid for a general distribution, we obtain via simple manipulations and along with (9) and (17)

$$f_-(\sigma) = \sqrt{\frac{\langle \sigma^2 \rangle_+}{\langle \sigma^2 \rangle_-}} f_+\left( \sigma \sqrt{\frac{\langle \sigma^2 \rangle_+}{\langle \sigma^2 \rangle_-}} \right). \tag{20}$$

## III. LIQUID-GAS PHASE EQUILIBRIUM OF THE POLYDISPERSE EXTENSION OF THE 1:1 PRIMITIVE MODEL FOR ELECTROLYTES

Above we have extended the MSNC approach to a polydisperse CHS fluid. In the following we shall focus on the generalized 1:1 primitive model for an electrolyte, which in the MSNC framework consists of a polydisperse mixture of neutral dimers, each formed by two oppositely charged hard spheres; the dimers are thus polar. Thermodynamic properties, which are needed to calculate the phase diagram of such a fluid of dimers can readily be obtained via the PMSA.[21] This concept will be introduced in the following, first for the multicomponent mixture and then generalized to the polydisperse mixture.

### A. PMSA thermodynamics for the multicomponent polar hard-sphere dimer fluid

Again, we start with a discrete version of the model. We consider an $(M/2)$-component mixture of dimers in which each dimer is built up of two tangentially bonded charged hard spheres with charges $ez_\alpha^a$ and diameters $\sigma_\alpha^a$. Here the index $a$ denotes the species of the dimer and the index $\alpha$, which takes the values + or −, characterizes the positively or negatively charged hard-sphere site of the dimer; due to charge neutrality, $ez_+^a = -ez_-^a$. The number density of each dimer species in the system is $\rho^a = N^a/V$, where $N^a$ is the number of dimers of type $a$.

The concept of PMSA for this model is based on the generalization of the Ornstein-Zernike equation, which reads in $k$ space[21]

$$\hat{\mathbf{h}}_{\alpha\beta}^{ab}(k) = \hat{\mathbf{c}}_{\alpha\beta}^{ab}(k) + \sum_c \rho^c \sum_\gamma \hat{\mathbf{c}}_{\alpha\gamma}^{ac}(k) \boldsymbol{\alpha} \hat{\mathbf{h}}_{\gamma\beta}^{cb}(k), \tag{21}$$

along with the PMSA closure relations

$$\begin{aligned} \mathbf{c}_{\alpha\beta}^{ab}(r) &= -\mathbf{E}\beta\Phi_{\alpha\beta}^{ab}(r) + \frac{\mathbf{t}_{\alpha\beta}^{ab}}{2\pi\sigma_{\alpha\beta}^{ab}} \delta(r - \sigma_{\alpha\beta}^{ab}), \quad r > \sigma_{\alpha\beta}^{ab}, \\ \mathbf{h}_{\alpha\beta}^{ab}(r) &= -\mathbf{E}, \quad r < \sigma_{\alpha\beta}^{ab}, \end{aligned} \tag{22}$$

where $\sigma_{\alpha\beta}^{ab} = \frac{1}{2}(\sigma_\alpha^a + \sigma_\beta^b)$; $\hat{\mathbf{h}}_{\alpha\beta}^{ab}(k)$ and $\hat{\mathbf{c}}_{\alpha\beta}^{ab}(k)$ are matrices whose elements are the Fourier transforms of the corresponding matrices in $r$-space $\mathbf{h}_{\alpha\beta}^{ab}(r)$ and $\mathbf{c}_{\alpha\beta}^{ab}(r)$,

$$\mathbf{h}_{\alpha\beta}^{ab}(r) = \begin{pmatrix} h_{\alpha_0\beta_0}^{ab}(r) & h_{\alpha_0\beta_A}^{ab}(r) & h_{\alpha_0\beta_B}^{ab}(r) \\ h_{\alpha_A\beta_0}^{ab}(r) & h_{\alpha_A\beta_A}^{ab}(r) & h_{\alpha_A\beta_A}^{ab}(r) \\ h_{\alpha_B\beta_0}^{ab}(r) & h_{\alpha_B\beta_A}^{ab}(r) & h_{\alpha_B\beta_B}^{ab}(r) \end{pmatrix},$$

$$\mathbf{c}_{\alpha\beta}^{ab}(r) = \begin{pmatrix} c_{\alpha_0\beta_0}^{ab}(r) & c_{\alpha_0\beta_A}^{ab}(r) & c_{\alpha_0\beta_B}^{ab}(r) \\ c_{\alpha_A\beta_0}^{ab}(r) & c_{\alpha_A\beta_A}^{ab}(r) & c_{\alpha_A\beta_B}^{ab}(r) \\ c_{\alpha_B\beta_0}^{ab}(r) & c_{\alpha_B\beta_A}^{ab}(r) & c_{\alpha_B\beta_B}^{ab}(r) \end{pmatrix}.$$

The matrices $\mathbf{t}_{\alpha\beta}^{ab}$, $\boldsymbol{\alpha}$, and $\mathbf{E}$ occurring in the above expressions are defined as follows:

$$(\mathbf{t}_{\alpha\beta}^{ab})_{KL} = t_{\alpha_K\beta_L}^{ab} = \frac{\delta_{ab}}{2\rho^a} [\delta_{KA}\delta_{LB}\delta_{\alpha-}\delta_{\beta+} + \delta_{KB}\delta_{LA}\delta_{\alpha+}\delta_{\beta-}],$$

$$(\boldsymbol{\alpha})_{KL} = \alpha_{KL} = 1 - \delta_{KL} + \delta_{0K}\delta_{0L},$$

$$(\mathbf{E})_{KL} = E_{KL} = \delta_{0K}\delta_{0L}.$$

Here the subindices $K$ and $L$ can take each the values 0, $A$, and $B$, and characterize the bonding states of the corresponding particle:[21] 0 denotes the unbonded state and $A$ and $B$ denote the $A$-bonded and $B$-bonded states, respectively. The partial total correlation functions $h_{\alpha_K\beta_L}^{ab}(r)$ are related to the site-site total correlation functions $h_{\alpha\beta}^{ab}(r)$ via

$$h_{\alpha\beta}^{ab}(r) = \sum_{KL} h_{\alpha_K\beta_L}(r). \tag{23}$$

Since the explicit solution of the PMSA has been derived earlier[21] for the most general case of a multicomponent mixture of charged hard-sphere flexible chain molecules, we will skip here further details and present in the following only the final expressions, specified for the model in question. Similar as in the case of the "conventional" MSA for a multicomponent mixture of CHS,[7,8] the solution of the PMSA (Ref. 21) can be reduced to the solution of one single nonlinear algebraic equation for the so-called scaling parameter $\Gamma$ introduced by Blum[7] and Blum and Høye.[8] In an effort to guarantee formal consistency we stick in the present contribution exactly to the same nomenclature as introduced in Ref. 8;

note that therefore the index $n$ appearing in some of the subsequent expression has no relevance. In the present case this equation takes the following form:

$$\Gamma^2 = \pi\beta^* \sum_{a=1}^{M/2} \rho^a \left\{ \sum_\alpha \left[ \Gamma_\alpha^a \left( z_\alpha^a - \frac{\pi(\sigma_\alpha^a)^2 \tilde{P}_n}{2\Delta + \pi\tilde{\Omega}_n} \right) \right]^2 + \frac{\Gamma_+^a \Gamma_-^a}{\sigma_{+-}^{aa}} \sum_\alpha (\sigma_\alpha^a \Gamma_\alpha^a) \prod_\alpha \left( z_\alpha^a - \frac{\pi(\sigma_\alpha^a)^2 \tilde{P}_n}{2\Delta + \pi\tilde{\Omega}_n} \right) \right\}, \tag{24}$$

where we have introduced $\beta^* = -e\beta/\epsilon$ and $\Delta = 1 - \pi\zeta_3/6$,

$$\Gamma_\alpha^a = (1 + \sigma_\alpha^a \Gamma)^{-1}, \tag{25}$$

$$\zeta_m = \sum_{a=1}^{M/2} \rho^a \sum_\alpha (\sigma_\alpha^a)^m, \quad m = 1,2,3, \tag{26}$$

$$\tilde{P}_n = \sum_{a=1}^{M/2} \rho^a \left\{ \sum_\alpha \sigma_\alpha^a z_\alpha^a \Gamma_\alpha^a + \frac{\Gamma_+^a \Gamma_-^a}{2\sigma_{+-}^{aa}} [(\sigma_+^a)^2 z_-^a + (\sigma_-^a)^2 z_+^a] \right\}, \tag{27}$$

and

$$\tilde{\Omega}_n = \sum_{a=1}^{M/2} \rho^a \left[ \sum_\alpha (\sigma_\alpha^a)^3 \Gamma_\alpha^a + \frac{(\sigma_+^a)^2 (\sigma_-^a)^2}{\sigma_{+-}^{aa}} \Gamma_+^a \Gamma_-^a \right]. \tag{28}$$

Hereafter we are using the notation $\Sigma_\alpha (\ldots)_\alpha = (\ldots)_- + (\ldots)_+$.

Once we know the scaling parameter $\Gamma$ we can calculate all the thermodynamic properties of the model. Following Bernard and Blum,[34,35] one finds

$$\beta \frac{U^{\mathrm{el}}}{V} = -\beta^* \left\{ \sum_{a=1}^{M/2} \rho^a \left[ \Gamma \sum_\alpha (z_\alpha^a)^2 \Gamma_\alpha^a - \frac{z_+^a z_-^a \Gamma_+^a \Gamma_-^a}{\sigma_{+-}^{aa}} \right] + \frac{\pi \tilde{P}_n^2}{2\Delta + \pi\tilde{\Omega}_n} \right\}, \tag{29}$$

$$\beta A = \beta A^{\mathrm{ref}} + \beta U^{\mathrm{el}} + \frac{\Gamma^3}{3\pi}, \tag{30}$$

and

$$\beta P \frac{V}{N^d} = \beta P^{\mathrm{ref}} \frac{V}{N^d} - \frac{2\Gamma^3}{3\pi\zeta_0} - \frac{4\beta^*}{\pi\zeta_0} \left( \frac{\pi \tilde{P}_n}{2\Delta + \pi\tilde{\Omega}_n} \right)^2, \tag{31}$$

where $U^{\mathrm{el}}$ is the electrostatic contribution to the internal energy, $A$ is the Helmholtz free energy, and $P$ is the pressure. The superscript "ref" denotes the corresponding properties of the reference system (see below), $N^d$ is the total number of dimers in the system, $N^d = \Sigma_{a=1}^{M/2} N^a$. Expressions (29)–(31) represent the generalization of the corresponding expressions derived earlier[34] for a fluid of dimerizing CHS in the limit of complete association.

Using the standard relation between the free energy and chemical potential we find

$$\beta\mu^a = \beta \frac{\partial}{\partial \rho^a} \left( \frac{A}{V} \right) = \beta\mu^{a;\mathrm{ref}} + \beta\Delta\mu^{a;\mathrm{el}}, \tag{32}$$

where

$$\beta\Delta\mu^{a;\mathrm{el}} = -\beta^* \left\{ \Gamma \sum_\alpha (z_\alpha^a)^2 \Gamma_\alpha^a - \frac{z_+^a z_-^a}{\sigma_{+-}^{aa}} \Gamma_+^a \Gamma_-^a + \frac{\pi \tilde{P}_n}{2\Delta + \pi\tilde{\Omega}_n} \left[ 2 \frac{\partial \tilde{P}_n}{\partial \rho^a} - \frac{\pi \tilde{P}_n}{2\Delta + \pi\tilde{\Omega}_n} \times \left( \frac{\partial \tilde{\Omega}_n}{\partial \rho^a} - \frac{1}{3} \sum_\alpha (\sigma_\alpha^a)^3 \right) \right] \right\}, \tag{33}$$

with the explicit expressions for the partial derivatives,

$$\frac{\partial \tilde{P}_n}{\partial \rho_a} = \sum_\alpha (z_\alpha^a)^2 \Gamma_\alpha^a + \frac{\Gamma_+^a \Gamma_-^a}{2\sigma_{+-}^{aa}} [(\sigma_+^a)^2 z_-^a + (\sigma_-^a)^2 z_+^a], \tag{34}$$

$$\frac{\partial \tilde{\Omega}_n}{\partial \rho_a} = \sum_\alpha (\sigma_\alpha^a)^3 \Gamma_\alpha^a + \frac{(\sigma_+^a)^2 (\sigma_-^a)^2}{\sigma_{+-}^{aa}} \Gamma_+^a \Gamma_-^a. \tag{35}$$

For the reference system we use a fluid of uncharged hard-sphere dimers, whose properties can be calculated using Wertheim's thermodynamic perturbation theory (TPT).[31,32,36] According to this concept, the Helmholtz free energy of a fluid of hard-sphere dimers $A^{\mathrm{ref}}$ can be written as a sum over three terms,

$$A^{\mathrm{ref}} = A^{\mathrm{id}} + \Delta A^{\mathrm{hs}} + \Delta A^{\mathrm{ass}}, \tag{36}$$

where $A^{\mathrm{id}}$ is the ideal contribution to the free energy, $\Delta A^{\mathrm{hs}}$ is the excess free energy of the multicomponent hard-sphere fluid, representing a completely dissociated dimer fluid, and $\Delta A^{\mathrm{ass}}$ is the contribution due to the formation of the dimers, which is given by[36]

$$\beta \frac{\Delta A^{\mathrm{ass}}}{V} = -\sum_{a=1}^{M/2} \rho_a \ln g_{+-}^{aa}. \tag{37}$$

where $g_{+-}^{aa}$ is the contact value of the radial distribution function between the two uncharged hard spheres, $(+,a)$ and $(-,a)$, which form the dimer of species $a$ upon association. For the contact value of the hard-sphere fluid $g_{+-}^{aa}$ we have used the Percus-Yevick expression[8]

$$g_{+-}^{aa} = \frac{1}{\Delta} + \frac{\pi \sigma_+^a \sigma_-^a \zeta_2}{4\Delta^2 \sigma_{+-}^{aa}}. \tag{38}$$

The Helmholtz free energy is related to the pressure and the chemical potential via standard thermodynamic relations which now read

$$\beta P^{\mathrm{ref}} \frac{V}{N^d} = \rho^d \frac{\partial}{\partial \rho^d} \left( \frac{\beta A^{\mathrm{ref}}}{N^d} \right) = 1 + \beta\Delta P^{\mathrm{hs}} \frac{V}{N^d} + \beta\Delta P^{\mathrm{ass}} \frac{V}{N^d} \tag{39}$$

and

$$\mu^{a;\mathrm{ref}} = \frac{\partial}{\partial \rho^a} \left( \frac{A^{\mathrm{ref}}}{V} \right) = \mu^{a;\mathrm{id}} + \sum_\alpha \Delta\mu_\alpha^{a;\mathrm{hs}} + \Delta\mu^{a;\mathrm{ass}}, \tag{40}$$

where $\Delta P^{\mathrm{hs}}$ and $\Delta\mu_\alpha^{a;\mathrm{hs}}$ are contributions to the pressure and the chemical potential of hard-sphere particles with indices $(\alpha,a)$ of the multicomponent hard-sphere fluid, which represents a completely dissociated dimer fluid. For these quanti-

ties we have used the semiempirical expressions due to Mansoori *et al.*[37] Further,

$$\beta\Delta P^{\mathrm{ass}} = -\frac{1}{6}\pi\lambda_1\zeta_3 - \frac{1}{4}\pi\lambda_2\zeta_2\left(1+\frac{\pi}{3\Delta}\zeta_3\right), \tag{41}$$

$$\beta\Delta\mu^{a;\mathrm{ass}} = -\ln g_{+-}^{aa} - \frac{1}{6}\pi\lambda_1\sum_\alpha(\sigma_\alpha^a)^3 - \frac{1}{6}\pi\lambda_2\left[\frac{\pi}{2\Delta}\zeta_2\sum_\alpha(\sigma_\alpha^a)^3+\frac{3}{2}\sum_\alpha(\sigma_\alpha^a)^2\right], \tag{42}$$

with

$$\lambda_1 = \sum_{a=1}^{M/2}\rho^a\frac{\sigma_{+-}^{aa}}{\sigma_{+-}^{aa}\Delta+\frac{1}{4}\pi\sigma_+^a\sigma_-^a\zeta_2} \quad \text{and} \tag{43}$$

$$\lambda_2 = \sum_{a=1}^{M/2}\rho^a\frac{\sigma_+^a\sigma_-^a}{\sigma_{+-}^{aa}\Delta+\frac{1}{4}\pi\sigma_+^a\sigma_-^a\zeta_2}.$$

### B. PMSA thermodynamics for the polydisperse polar hard-sphere dimer fluid

Generalization of the above expressions for the thermodynamic properties from the multicomponent system to the polydisperse fluid is rather straightforward: again, we introduce the distribution function [$\mathcal{I}(\sigma,z)$ or $f_\pm(\sigma)$] and replace throughout summations over the discrete species index $a$ of a dimer by integrations over its continuous counterpart $\sigma$. The latter fixes, due to (17), the charge of the ions; as a consequence of relation (20) between $f_+(\sigma)$ and $f_-(\sigma)$, it is sufficient to specify the distribution function of either type of the ions. Without loss of generality we choose $f_+(\sigma)$, which now completely defines the polydisperse polar dimer fluid we want to study. From (17) we find that the diameters of the two sites of each dimer are related via

$$\frac{\sigma_-}{\sigma_+} = \sqrt{\frac{\langle\sigma^2\rangle_-}{\langle\sigma^2\rangle_+}}. \tag{44}$$

This functional relation, $\sigma_-=\sigma_-(\sigma_+)$, will be used implicitly in the subsequent expressions.

With all these in mind, Eqs. (24)–(28) become

$$\Gamma^2 = \pi\beta^*\rho_+\int_0^\infty d\sigma_+ f_+(\sigma_+)\times\left\{\sum_\alpha\left[\Gamma_\alpha(\sigma_\alpha)\left(z_\alpha-\frac{\pi(\sigma_\alpha)^2\widetilde{P}_n}{2\Delta+\pi\widetilde{\Omega}_n}\right)\right]^2 + \frac{2\Gamma_+(\sigma_+)\Gamma_-(\sigma_-)}{\sigma_++\sigma_-}\times\prod_\alpha\left(z_\alpha-\frac{\pi(\sigma_\alpha)^2\widetilde{P}_n}{2\Delta+\pi\widetilde{\Omega}_n}\right)\sum_\alpha\sigma_\alpha\Gamma_\alpha(\sigma_\alpha)\right\}, \tag{45}$$

where $\rho_+=\rho/2$ and $\Gamma_\alpha(\sigma_\alpha)=(1+\sigma_\alpha\Gamma)^{-1}$ and $\Delta$ as defined above; further,

$$\zeta_m = \rho_+\int_0^\infty d\sigma_+ f_+(\sigma_+)\sum_\alpha(\sigma_\alpha)^m, \quad m=1,2,3, \tag{46}$$

$$\widetilde{P}_n = \rho_+\int_0^\infty d\sigma_+ f_+(\sigma_+)\left\{\sum_\alpha\sigma_\alpha z_\alpha\Gamma_\alpha(\sigma_\alpha) + \frac{\Gamma_+(\sigma_+)\Gamma_-(\sigma_-)}{\sigma_++\sigma_-}[(\sigma_+)^2z_- + (\sigma_-)^2z_+]\right\}, \tag{47}$$

and

$$\widetilde{\Omega}_n = \rho_+\int_0^\infty d\sigma_+ f_+(\sigma_+)\left[\sum_\alpha(\sigma_\alpha)^3\Gamma_\alpha(\sigma_\alpha) + \frac{2(\sigma_+)^2(\sigma_-)^2}{\sigma_++\sigma_-}\Gamma_+(\sigma_+)\Gamma_-(\sigma_-)\right]. \tag{48}$$

The corresponding generalizations of the expressions for the internal energy (29) and the chemical potential (32) read

$$\beta\frac{U^{\mathrm{el}}}{V} = -\beta^*\left\{\rho_+\int_0^\infty d\sigma_+ f_+(\sigma_+)\left[\Gamma\sum_\alpha(z_\alpha)^2\Gamma_\alpha(\sigma_\alpha) - \frac{2z_+z_-\Gamma_+(\sigma_+)\Gamma_-(\sigma_-)}{\sigma_++\sigma_-}\right]+\frac{\pi\widetilde{P}_n^2}{2\Delta+\pi\widetilde{\Omega}_n}\right\}, \tag{49}$$

$$\beta\mu(\sigma_+) = \beta\mu^{\mathrm{ref}}(\sigma_+) + \beta\Delta\mu^{\mathrm{el}}(\sigma_+); \tag{50}$$

in above expression for $\beta\mu^{\mathrm{ref}}(\sigma_+)$ we need the generalization of expression (42) for $\beta\Delta\mu^{\alpha;\mathrm{ass}}$ to the polydisperse case, which becomes

$$\beta\Delta\mu^{\mathrm{ass}}(\sigma_+) = -\ln\left[\frac{1}{\Delta}+\frac{\pi\sigma_+\sigma_-\zeta_2}{2\Delta^2(\sigma_++\sigma_-)}\right] - \frac{1}{6}\pi\left\{\lambda_1\sum_\alpha(\sigma_\alpha)^3 + \lambda_2\left[\frac{\pi}{2\Delta}\zeta_2\sum_\alpha(\sigma_\alpha)^3+\frac{3}{2}\sum_\alpha(\sigma_\alpha)^2\right]\right\}, \tag{51}$$

with

$$\lambda_1 = \rho_+\int_0^\infty d\sigma_+ f_+(\sigma_+)\frac{\sigma_++\sigma_-}{(\sigma_++\sigma_-)\Delta+\frac{1}{2}\pi\sigma_+\sigma_-\zeta_2}, \tag{52}$$

$$\lambda_2 = \rho_+\int_0^\infty d\sigma_+ f_+(\sigma_+)\frac{2\sigma_+\sigma_-}{(\sigma_++\sigma_-)\Delta+\frac{1}{2}\pi\sigma_+\sigma_-\zeta_2}, \tag{53}$$

and

$$\beta\Delta\mu^{\mathrm{el}}(\sigma_+) = -\beta^*\left\{\Gamma\sum_\alpha(z_\alpha)^2\Gamma_\alpha(\sigma_\alpha) - \frac{2z_+z_-}{\sigma_++\sigma_-}\Gamma_+(\sigma_+)\Gamma_-(\sigma_-) + \frac{\pi\widetilde{P}_n}{2\Delta+\pi\widetilde{\Omega}_n}\left[2\frac{\delta\widetilde{P}_n}{\delta f(\sigma_+)}\right.\right.$$

$$-\frac{\pi\tilde{P}_n}{2\Delta+\pi\tilde{\Omega}_n}\left(\frac{\delta\tilde{\Omega}_n}{\delta f(\sigma_+)}-\frac{1}{3}\sum_\alpha(\sigma_\alpha^a)^3\right)\Bigg]\Bigg\}, \tag{54}$$

with the explicit expressions for the functional derivatives,

$$\frac{\delta\tilde{P}_n}{\delta f(\sigma_+)}=\sum_\alpha(z_\alpha)^2\Gamma_\alpha(\sigma_\alpha)+\frac{\Gamma_+(\sigma_+)\Gamma_-(\sigma_-)}{\sigma_++\sigma_-}\times[(\sigma_+)^2z_-+(\sigma_-)^2z_+] \tag{55}$$

and

$$\frac{\delta\tilde{\Omega}_n}{\delta f(\sigma_+)}=\sum_\alpha(\sigma_\alpha)^3\Gamma_\alpha(\sigma_\alpha)+\frac{2(\sigma_+)^2(\sigma_-)^2}{\sigma_++\sigma_-}\Gamma_+(\sigma_+)\Gamma_-(\sigma_-). \tag{56}$$

For the pressure the expression for the polydisperse version coincides with the one of the multicomponent case (31); the only difference becomes visible in the expressions for the generalized moments $\zeta_m$, $\tilde{P}_n$, $\tilde{\Omega}_n$, $\lambda_1$, and $\lambda_2$: in the polydisperse case they are now defined by relations (46)–(48), (52), and (53), respectively. The thermodynamic properties of the polydisperse hard-sphere reference fluid, $\Delta P^{\mathrm{hs}}$ and $\Delta\mu^{\mathrm{hs}}(\sigma_\alpha)$, that are required in the expressions for the pressure (39) and for the chemical potential (40), are generalizations of the semiempirical expressions due to Mansoori *et al.*[37] to the polydisperse case.[6,38]

### C. Phase equilibrium

In this contribution we focus on two-phase equilibria, when at a given temperature $T$ the parent phase, characterized by the distribution function $f_+^{(0)}(\sigma)$ and the number density $\rho_+^{(0)}$, separates into two coexisting daughter phases, with the distribution functions $f_+^{(1)}(\sigma)$ and $f_+^{(2)}(\sigma)$ and densities $\rho_+^{(1)}$ and $\rho_+^{(2)}$; the properties of the species with index "−" can be calculated from these quantities via the relations presented in the preceding section. Hereafter superscripts 0, 1, and 2 denote the properties of the respective phases. Phase equilibrium conditions include (i) conservation of the total volume of the system, (ii) conservation of the total number of the particles of each species, (iii) equality of the chemical potentials of particles of the same species in the coexisting phases, and (iv) equality of the pressure in the coexisting phases.

The first two conditions lead to the following relation between the distribution functions of the coexisting phases:[5,39]

$$\rho_+^{(2)}f_+^{(2)}(\sigma_+)=\frac{\rho_+^{(1)}-\rho_+^{(2)}}{\rho_+^{(1)}-\rho_+^{(0)}}\rho_+^{(0)}f_+^{(0)}(\sigma_+)+\frac{\rho_+^{(0)}-\rho_+^{(0)}}{\rho_+^{(0)}-\rho_+^{(1)}}\rho_+^{(1)}f_+^{(1)}(\sigma_+). \tag{57}$$

A further relation between $f_+^{(1)}(\sigma_+)$ and $f_+^{(2)}(\sigma_+)$ follows from the equality of the chemical potentials, i.e., condition (iii),

$$f_+^{(1)}(\sigma_+)=f_+^{(2)}(\sigma_+)\frac{\rho_+^{(2)}}{\rho_+^{(1)}}\exp[\beta\Delta\mu^{\mathrm{ex}}], \tag{58}$$

where

$$\Delta\mu^{\mathrm{ex}}=\mu^{\mathrm{ex}}(\sigma_+T;\rho_+^{(2)},[f_+^{(2)}])-\mu^{\mathrm{ex}}(\sigma_+,T;\rho_+^{(1)},[f_+^{(1)}]), \tag{59}$$

where the superscript "ex" denotes the excess (over ideal gas) value of the chemical potential and the square brackets indicate functional dependencies. Eliminating from these two relations either $f_+^{(2)}(\sigma_+)$ or $f_+^{(1)}(\sigma_+)$ we get

$$f_+^{(k)}(\sigma_+)=f_+^{(0)}(\sigma_+)Q^{(k)}(\sigma_+,T,\rho_+^{(0)};\rho_+^{(1)},\rho_+^{(2)},[f_+^{(k)}(\sigma_+)]),\quad k=1,2, \tag{60}$$

where

$$\rho_+^{(k)}Q^{(k)}(\sigma_+,T,\rho_+^{(0)};\rho_+^{(1)},\rho_+^{(2)},[f_+^{(k)}(\sigma_+)])=\frac{\rho_+^{(0)}(\rho_+^{(2)}-\rho_+^{(1)})\{1-\delta_{1k}[1-\exp(\beta\Delta\mu^{\mathrm{ex}})]\}}{(\rho_+^{(0)}-\rho_+^{(1)})-(\rho_+^{(0)}-\rho_+^{(2)})\exp(\beta\Delta\mu^{\mathrm{ex}})}. \tag{61}$$

Equation (60) contains three unknown quantities, i.e., $\rho^{(1)+}$, $\rho_+^{(2)}$, and either $f_+^{(1)}(\sigma_+)$ or $f_+^{(2)}(\sigma_+)$. Additional two equations, which involve these yet undetermined parameters, follow from the equality of the pressure in the two phases

$$P(T;\rho_+^{(1)},[f_+^{(1)}])=P(T;\rho_+^{(2)},[f_+^{(2)}]) \tag{62}$$

and from the normalizing conditions

$$\int_0^\infty d\sigma_+f_+^{(k)}(\sigma_+)=1,\quad k=1,2. \tag{63}$$

Relations (60), (62), and (63) represent a closed set of equations for the unknown densities $\rho_+^{(k)}$ and the unknown functions $f_+^{(k)}(\sigma_+)$ with $k=1,2$; however, their direct solution is from the numerical point of view in practice not feasible, since they have to be solved for each of the infinitely many values of $\sigma_+$.

From the analysis presented in Sec. III B it becomes obvious that polydisperse mixtures of polar hard-sphere dimers treated within the PMSA belong to the class of truncatable free-energy models,[4] this means that their thermodynamic properties can be presented in terms of a finite number of generalized moments of the distribution function, $f_+(\sigma_+)$. Thus the phase equilibrium conditions for the system presented above can be mapped onto a finite set of coupled nonlinear equations in those moments. Since this concept has been discussed at length in earlier contributions and was applied to several different models[5,38–41] we will skip here the details and present only a brief summary of the method.

In the present case we have a set of 18 algebraic equations for the 14 generalized moments $\zeta_m^{(k)}$, $\lambda_1^{(k)}$, $\lambda_2^{(k)}$, $\tilde{P}_n^{(k)}$, and $\tilde{\Omega}_n^{(k)}$ (with $k=1,2$ and $m=1,2,3$), for the two densities $\rho_+^{(1)}$ and $\rho_+^{(2)}$, and for the two coupling parameters of the two coexisting phases $\Gamma^{(1)}$ and $\Gamma^{(2)}$. Using relation (60) together with the definitions of the moments, (46)–(48), (52), and (53), and dropping for simplicity for the moment the long list of arguments in the $Q^{(k)}$, by putting

$$Q^{(k)}\equiv Q^{(k)}(\sigma_+,T,\rho_+^{(0)};\rho_+^{(1)},\rho_+^{(2)},[\Gamma^{(1)},\{\zeta\lambda\tilde{P}_n\tilde{\Omega}_n\}^{(1)}],[\Gamma^{(2)},\{\zeta\lambda\tilde{P}_n\tilde{\Omega}_n\}^{(2)}]), \tag{64}$$

we obtain the following 14 equations:

$$\zeta_m^{(k)} = \rho_+^{(k)} \int_0^\infty d\sigma_+ f_+^{(0)}(\sigma_+) Q^{(k)} \sum_\alpha (\sigma_\alpha)^m, \quad m = 1,2,3, \quad (65)$$

$$\tilde{P}_n^{(k)} = \rho_+^{(k)} \int_0^\infty d\sigma_+ f_+^{(0)}(\sigma_+) Q^{(k)} \left\{ \sum_\alpha \sigma_\alpha z_\alpha \Gamma_\alpha^{(k)}(\sigma_\alpha) + \frac{\Gamma_+^{(k)}(\sigma_+)\Gamma_-^{(k)}(\sigma_-)}{\sigma_+ + \sigma_-} [(\sigma_+)^2 z_- + (\sigma_-)^2 z_+] \right\}, \quad (66)$$

$$\tilde{\Omega}_n^{(k)} = \rho_+^{(k)} \int_0^\infty d\sigma_+ f_+^{(0)}(\sigma_+) Q^{(k)} \left[ \sum_\alpha (\sigma_\alpha)^3 \Gamma_\alpha^{(k)}(\sigma_\alpha) + \frac{2\sigma_+^2\sigma_-^2}{\sigma_+ + \sigma_-} \Gamma_+^{(k)}(\sigma_+)\Gamma_-^{(k)}(\sigma_-) \right], \quad (67)$$

$$\lambda_1^{(k)} = \rho_+^{(k)} \int_0^\infty d\sigma_+ f_+^{(0)} \times (\sigma_+) Q^{(k)} \frac{\sigma_+ + \sigma_-}{(\sigma_+ + \sigma_-)\Delta^{(k)} + \frac{1}{2}\pi\sigma_+\sigma_-\zeta_2^{(k)}}, \quad (68)$$

$$\lambda_2^{(k)} = \rho_+^{(k)} \int_0^\infty d\sigma_+ f_+^{(0)} \times (\sigma_+) Q^{(k)} \frac{2\sigma_+\sigma_-}{(\sigma_+ + \sigma_-)\Delta^{(k)} + \frac{1}{2}\pi\sigma_+\sigma_-\zeta_2^{(k)}}, \quad (69)$$

with $k=1,2$.

In the above notation the dependence on a set of parameters $[\Gamma^{(k)}, \{\zeta\lambda\tilde{P}_n\tilde{\Omega}_n\}^{(k)}]$ is equivalent to the functional dependence on $[f_+^{(k)}]$ and hereafter $\{\zeta\lambda\tilde{P}_n\tilde{\Omega}_n\}^{(k)}$ denotes the set of the moments $\zeta_m^{(k)}$, $\lambda_1^{(k)}$, $\lambda_2^{(k)}$, $\tilde{P}_n^{(k)}$, and $\tilde{\Omega}_n^{(k)}$.

The remaining four equations follow from the normalizing condition (63),

$$1 = \int_0^\infty d\sigma_+ f_+^{(0)}(\sigma_+) Q^{(k)}, \quad k = 1,2, \quad (70)$$

from the equality of the pressure in the coexisting phases (62),

$$P(T;\rho_+^{(1)},[\Gamma^{(1)},\{\zeta\lambda\tilde{P}_n\tilde{\Omega}_n\}^{(1)}]) = P(T;\rho_+^{(2)},[\Gamma^{(2)},\{\zeta\lambda\tilde{P}_n\tilde{\Omega}_n\}^{(2)}]), \quad (71)$$

and from the equation for the coupling parameter, written for each of the two coexisting phases,

$$[\Gamma^{(k)}]^2 = \pi\beta^*\rho_+^{(k)} \int_0^\infty d\sigma_+ f_+^{(0)}(\sigma_+) Q^{(k)} \times \left\{ \sum_\alpha \left[ \Gamma_\alpha^{(k)}(\sigma_\alpha) \left( z_\alpha - \frac{\pi\sigma_\alpha^2 \tilde{P}_n^{(k)}}{2\Delta^{(k)} + \pi\tilde{\Omega}_n^{(k)}} \right) \right]^2 + \frac{2\Gamma_+^{(k)}(\sigma_+)\Gamma_-^{(k)}(\sigma_-)}{\sigma_+ + \sigma_-} \times \prod_\alpha \left( z_\alpha - \frac{\pi\sigma_\alpha^2 \tilde{P}_n^{(k)}}{2\Delta^{(k)} + \pi\tilde{\Omega}_n^{(k)}} \right) \sum_\alpha \sigma_\alpha \Gamma_\alpha^{(k)}(\sigma_\alpha) \right\}. \quad (72)$$

Solution of the set of equations (65)–(72) at a given temperature $T$, density $\rho_+^{(0)}$, and distribution function $f_+^{(0)} \times(\sigma_+)$ of the parent phase yields the coexistence densities $\rho_+^{(k)}$ and distribution functions $f_+^{(k)}(\sigma_+)$ of the two daughter phases $(k=1,2)$.

In the general case of an arbitrary density $\rho_+^{(0)}$, the binodal lines will be terminated at a given temperature in two points, each of them corresponding to two densities. One of these densities (which is the coexistence density of one of the daughter phases) is equal to the density of the parent phase $\rho_+^{(0)}$. The set of these binodal terminal points determined at different values of $\rho_+^{(0)}$ forms the so-called cloud and shadow curves; by definition they represent the densities of the coexisting phases with an infinitely small amount of one phase emerging (shadow phase). The distribution function of the phase where the density is equal to the density of the parent phase (cloud phase) coincides—by definition—with $f^{(0)}(\sigma_+)$. Thus the cloud and shadow curves can be obtained as special or particular solutions of the general phase coexistence problem, when the generalized moments of one phase are equal to those of the parent phase. Only if $\rho_+^{(0)}$ is equal to the critical density, the two binodal lines meet at a critical point.

The numerical solution of the set of equations (65)–(72) was realized using a Newton-Raphson method. For the initial values of the unknowns we have used the corresponding quantities that we had obtained from the solution of the bidisperse case;[19] calculations were started at relatively high temperatures and for a low degree of polydispersity. The final solution is then obtained by gradually lowering the temperature and by increasing the polydispersity to the desired values.

## IV. DISCUSSION

### A. The distribution functions

Similar as in Ref. 38 and for reasons explained there (Sec. II C) we have chosen for the distribution functions $f_\pm^{(0)}(\sigma)$ of the mother phase beta distributions, given by[42]

$$f_\pm^{(0)}(\sigma) = \frac{1}{\sigma_\pm^{(\max)}} \frac{1}{B(\gamma_\pm,\nu_\pm)} \times \left( \frac{\sigma}{\sigma_\pm^{(\max)}} \right)^{\gamma_\pm - 1} \left( 1 - \frac{\sigma}{\sigma_\pm^{(\max)}} \right)^{\nu_\pm - 1} \times \Theta(\sigma_\pm^{(\max)} - \sigma)\Theta(\sigma), \quad (73)$$

where $\Theta(x)$ is the Heaviside step function, $B(\gamma_\pm,\nu_\pm)$ is the beta function,[43] and $\gamma_\pm$ and $\nu_\pm$ are related to the first $(\sigma_\pm^{(0)} = \langle\sigma\rangle_\pm^{(0)})$ and to the second $(\langle\sigma^2\rangle_\pm^{(0)})$ moments by

$$\gamma_\pm = \frac{\sigma_\pm^{(\max)} - \sigma_\pm^{(0)}(1 + D_\pm^{(0)})}{\sigma_\pm^{(\max)} D_\pm^{(0)}}, \quad (74)$$

$$\nu_{\pm} = \left( \frac{\sigma_{\pm}^{(\max)} - \sigma_{\pm}^{(0)}}{\sigma_{\pm}^{(0)}} \right) \gamma_{\pm}, \tag{75}$$

with

$$D_{\pm}^{(0)} = \langle \sigma^2 \rangle_{\pm}^{(0)} / (\langle \sigma \rangle_{\pm}^{(0)})^2 - 1; \tag{76}$$

according to (20) the parameters $\sigma_{\pm}^{(\max)}$ are not independent, i.e., $\sigma_{-}^{(\max)} = \sigma_{+}^{(\max)}/K$, where $K$ is

$$K = \frac{\sigma_{+}^{(0)}}{\sigma_{-}^{(0)}} \sqrt{\frac{1 + D_{+}^{(0)}}{1 + D_{-}^{(0)}}}. \tag{77}$$

Once we have determined the daughter distribution functions, $f_{\pm}^{(k)}(\sigma)$, $k=1,2$,—see below—we shall determine, likewise, first and second moments which we denote by $\langle \sigma \rangle_{\pm}^{(k)}$ and $\langle \sigma^2 \rangle_{\pm}^{(k)}$, $k=1,2$; in the figures we shall display $D_{\pm}^{(k)}$, which is then calculated according to (76). Even though the daughter distribution functions $f_{\pm}^{(k)}(\sigma)$ will certainly not be beta distributions, we have proposed in Ref. 5 a procedure that analyzes the shapes of the $f_{\pm}^{(k)}(\sigma)$ in terms of the "closest" beta distributions $f_{\pm}^{(k);\mathrm{beta}}(\sigma)$—for further details we refer to Ref. 5. These functions will be displayed in the following graphs along with the $f_{\pm}^{(k)}(\sigma)$.

### B. The systems

Unfortunately computer simulation results for polydisperse CHS mixture which we might be used to test the accuracy of our approach are currently not available. We therefore start to compare the *predictions* for the critical parameters calculated with our approach with the corresponding values obtained via Monte Carlo (MC) simulations for the 1:1 primitive model for the electrolyte with size asymmetry:[12,13] this bidisperse model can be considered as a limiting case of our polydisperse CHS mixture where the width parameters $D_{\pm}^{(0)}$ of the distribution functions $f_{\pm}^{(0)}(\sigma)$ tend towards zero, i.e., $D_{\pm}^{(0)} \to 0$, and the $f_{\pm}^{(0)}(\sigma)$ reduce to the corresponding Dirac delta functions. We consider this comparison as very important since it allows us to estimate the limits of applicability of our approach.

Next we proceed to polydisperse CHS mixtures, which are now characterized by a *finite* degree of polydispersity, and consider two different systems:

(i) the first system, labeled as "I," is a polydisperse (size-) symmetric CHS mixture, which can be considered as a generalization of the size-symmetric primitive model for electrolytes to the polydisperse case, thus $\sigma_{-}^{(0)} = \sigma_{+}^{(0)}$;

(ii) the second system, labeled as "II," is a polydisperse mixture of CHS which is asymmetric in size; it can be considered as a polydisperse extension of the 1:1 primitive model for electrolytes with an asymmetry in the size of the HS particles; here we chose $\sigma_{-}^{(0)} = 0.7\sigma_{+}^{(0)}$.

All our numerical calculations for systems I and II were carried out using the distribution functions $f_{\pm}^{(0)}(\sigma)$ introduced above with $\sigma_{+}^{(\max)} = 2\sigma_{+}^{(0)}$, $D_{\pm}^{(0)} = 0.01$, and $|\langle z_{\pm}^{(0)} \rangle| = 1$.

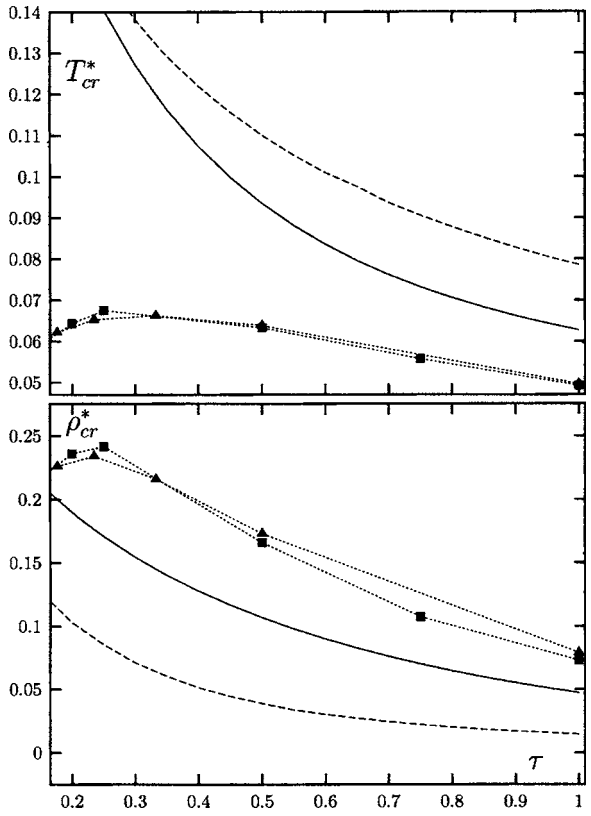


FIG. 1. Critical temperature $T_{\mathrm{cr}}^*$ (top) and critical density $\rho_{\mathrm{cr}}^*$ (bottom) vs $\tau = \sigma_{-}^{(0)}/\sigma_{+}^{(0)}$ for the bidisperse size-asymmetric 1:1 primitive model for electrolytes, as predicted by MSA (dashed lines), PMSA (solid lines) and MC simulations [filled triangles (Ref. 12) and filled squares (Ref. 13)]. The dotted lines connecting the symbols are shown to guide the eye.

In what follows, the temperature $T$ and the densities $\rho$ of the system will be expressed by the dimensionless quantities $T^* = kT\sigma_{+}^{(0)}\epsilon/e^2$ and $\rho^* = \rho(\sigma_{+}^{(0)})^3$, respectively. The quantities we calculate are characterized by an upper index $k$ which assumes values of 1 and 2 and specifies the daughter phases which are fixed as follows: index "1" will refer to the low-density (gas) phase, while index "2" will refer to the high-density (fluid) phase. Further we introduce the size ratio $\tau = \sigma_{-}^{(0)}/\sigma_{+}^{(0)}$.

### C. Results

#### *1. Results for the bidisperse mixture of CHS*

In Fig. 1 we display the predictions for the critical parameters $T_{\mathrm{cr}}^*$ and $\rho_{\mathrm{cr}}^*$ of the size-asymmetric 1:1 primitive model for electrolytes obtained via the MSA, the PMSA, and via MC simulations for different degrees of size asymmetry $\tau$. On a quantitative level, both MSA and PMSA fail with respect to the simulation data; this is well documented in the literature[12,13] and therefore not surprising. In the range of $0.6 \lesssim \tau \lesssim 1$, MSA fails in the critical temperature by a factor of $\sim 1.6$ and in the critical density by $\sim 0.2$. The fact that the corresponding factors for the PMSA data are distinctively closer to 1 (i.e., $\sim 1.3$ for the temperature and $\sim 0.6$ for the densities) indicates that PMSA brings along a substantial improvement over the MSA it is able to grasp (at least partly) the complex scenarios encountered close to the critical point in the RPM—but certainly not in full detail. On a *qualitative*

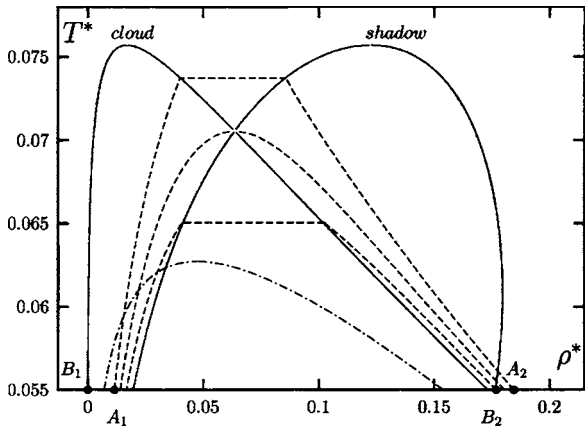


FIG. 2. Phase diagram ($T^*$ vs $\rho^*$) of the size-symmetric polydisperse CHS mixture (system I) specified in the text. Cloud and shadow curves are represented by the solid lines (as labeled), binodals by the broken lines: the values of the densities of the respective parent phase $\rho^{*(0)}$ can be identified from the intersection of the binodal with the cloud curve: $\rho^{*(0)}=0.04$, 0.1, and 0.0639 (critical binodal). Two pairs of points ($A_k$ and $B_k$, $k=1,2$) are chosen on the two $[\rho^{*(0)}=0.04]$ binodals and on the cloud and shadow curves which are specified in Table I. The dash-dotted line denotes the binodal curve for a size-symmetric (bidisperse) primitive model for electrolytes [with diameters $\sigma_+^{(0)}=\sigma_-^{(0)}$] treated within the PMSA (Ref. 19).

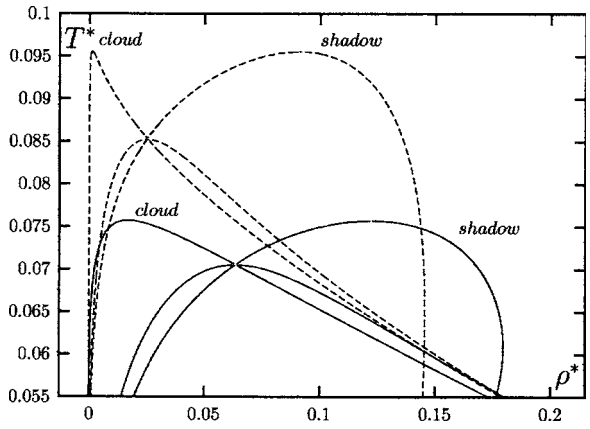


FIG. 3. Comparison of the phase diagrams (in terms of the cloud and shadow curves and the critical binodals) for the size-symmetric polydisperse CHS mixture (system I) calculated via the MSA (Ref. 5) (dashed lines) and the PMSA (solid lines).

level, both MSA and PMSA are able to describe the increase of $T^*_{\rm cr}$ and $\rho^*_{\rm cr}$, with decreasing size-asymmetry parameter $\tau$ for $\tau$ values down to $\sim 0.33$ and $\sim 0.23$, respectively. As $\tau$ is decreased further, simulations predict a decrease in $T^*_{\rm cr}$ and $\rho^*_{\rm cr}$, while the corresponding MSA and PMSA curves continue to increase.

We note that in earlier studies[12,13] it was concluded that MSA provides a qualitatively wrong dependence of the critical parameters on the size-asymmetry parameter $\tau$. In these contributions definitions for the reduced temperature and the reduced density were used which are different from the present one: $\tilde{T}^*=kT\left[\frac{1}{2}(1+\tau)\right]\sigma_+^{(0)}\epsilon/e^2$ and $\tilde{\rho}^*=\rho\left[\frac{1}{2}(1+\tau)\sigma_+^{(0)}\right]^3$. These definitions introduce an additional dependence of the critical parameters on $\tau$ via the factor $\frac{1}{2}(1+\tau)$ and are thus less appropriate for this analysis.

### 2. Results for system I

In Fig. 2 we present the phase diagram of the polydisperse system I which is size symmetric. We show the cloud and the shadow curves, along with three binodals for three selected densities, one of them begins the critical density, $\rho^*_{\rm cr}=0.0639$. The binodal curve for the size-symmetric (bidisperse) primitive model for electrolytes treated within the PMSA is shown for reference. On the binodal for $\rho^{*(0)}=0.04$ and on the cloud and shadow curves two pairs of points have been chosen (labeled $A_k$ and $B_k$, $k=1,2$) which are specified in Table I, for these pairs of state points the daughter distribution functions, $f_\pm^{(k)}(\sigma)$, $k=1,2$, are displayed in the subsequent Figs. 4 and 5 and are discussed in the text. In Fig. 3 we have redrawn the PMSA phase diagram of Fig. 2 (in terms of cloud and shadow curves and the critical binodal) and have compared these curves with the corresponding data obtained via the MSA reported in Ref. 5.

Compared to the bidisperse version of the system (Fig. 2) we find—similar as in the MSA—that the critical density and the critical temperature are shifted to larger values $[\rho^{*(\rm polydisp)}_{\rm cr;PMSA}/\rho^{*(\rm bidisp)}_{\rm cr;PMSA}\sim 1.35$ and $T^{*(\rm polydisp)}_{\rm cr;PMSA}/T^{*(\rm bidisp)}_{\rm cr;PMSA}\sim 1.12]$; however, with respect to the MSA,[5] this shift is more pronounced within PMSA. From Fig. 3 we learn that PMSA shifts the critical point—as desired—to larger $\rho^*$ values and to smaller $T^*$ values with respect to the MSA; the corresponding factors are $T^*_{\rm cr;MSA}/T^*_{\rm cr;PMSA}\sim 1.2$ and $\rho^*_{\rm cr;MSA}/\rho^*_{\rm cr;PMSA}\sim 0.4$. Consequently, the cloud curve and the binodal are much more symmetric within PMSA than within MSA.

We continue by discussing fractionation effects: at the level of the daughter distribution functions no considerable qualitative differences with respect to the MSA data[5] are observed; for completeness we display in Figs. 4 and 5 the daughter distribution functions $f_\pm^{(k)}(\sigma)$ of the two pairs of points ($A_k$ and $B_k$, $k=1,2$) specified in Fig. 2 and in Table I. Similar as observed for the MSA, the daughter distribution functions $f_\pm^{(k)}(\sigma)$ can be represented reasonably well by beta distributions, $f_\pm^{(k);\rm beta}(\sigma)$, $k=1,2$. The more quantitative information about fractionation can be obtained from the mean

TABLE I. Specification of selected pairs of points (index "1"—low-density gas phase, index "2"—high-density fluid phase) chosen in the phase diagram of the size-symmetric polydisperse CHS mixture (system I: points $A_k$ and $B_k$, $k=1,2$) indicated in Fig. 2 and of the size-asymmetric polydisperse CHS mixture (system II: points $C_k$, $k=1,2$) indicated in Fig. 8.

| System | Point | Localized on | $T^*$ | $\rho^{*(1)}$ | $\rho^{*(2)}$ |
|---|---|---|---|---|---|
| System I | $A_1$, $A_2$ | Binodal curve $[\rho^{*(0)}=0.04]$ | 0.055 | 0.0115 | 0.184 |
| | $B_1$, $B_2$ | Cloud and shadow curves | 0.055 | $0.189\times10^{-4}$ | 0.177 |
| System II | $C_1$, $C_2$ | Cloud and shadow curves | 0.055 | $0.113\times10^{-7}$ | 0.254 |

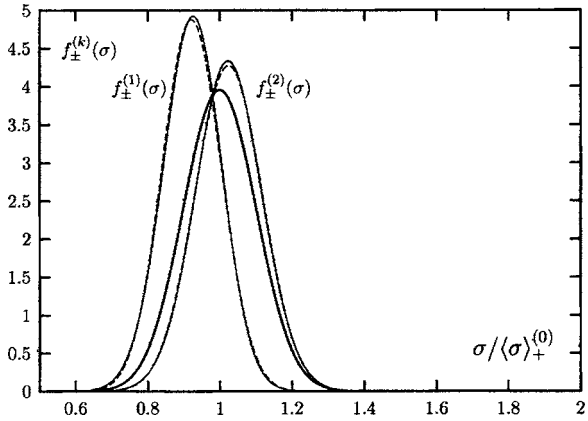


FIG. 4. Parent $[f_{\pm}^{(0)}(\sigma)]$ (thick full line) and daughter $[f_{\pm}^{(k)}(\sigma), k=1,2]$ distribution functions (full lines) for the size-symmetric polydisperse CHS mixture (system I) calculated for points $A_1$ and $A_2$, located on the $[\rho^{*(0)}=0.04]$ binodal in the phase diagram (see Table I and Fig. 2). Broken lines: $f_{\pm}^{(k);\text{beta}}(\sigma)$ as defined in the text. $k=1$—gas phase, $k=2$—fluid phase.

value (Fig. 6) and the width (Fig. 7) of the distribution functions of the daughter phases. The results for $\langle\sigma\rangle_{+}^{(k)}(=\langle\sigma\rangle_{-}^{(k)})$, $k=1,2$, show a similar behavior as in the MSA study (cf. Fig. 4 in Ref. 5), apart from the fact that the mean values of the daughter distribution functions vary now over a broader range. In contrast, the widths of the $f_{\pm}^{(k)}(\sigma)$ show a distinctively different behavior: while in the MSA the $D_{\pm}^{(k)}$ values of the daughter phases were always smaller than $D_{\pm}^{(0)}(=0.01)$, this is now different in the PMSA framework. Obviously, for densities below the critical density and for higher temperatures, $D_{\pm}^{(2)}$ can exceed in the fluid phase ($k=2$) the values of $D_{\pm}^{(0)}$, which means that for this parameter range the daughter distribution functions of the fluid phase is broadened. In addition, for $\rho^{*}<\rho_{\text{cr}}^{*}$, the curves for $D_{\pm}^{(k)}$ indicate that for lower temperatures the width of the daughter distribution functions is larger in the fluid phase than in the gas phase, while for higher temperatures, $D_{\pm}^{(1)}>D_{\pm}^{(2)}$, which causes a looplike shape of the $D_{\pm}^{(k)}$ curves (broken line in Fig. 7). A particularly nonmonotonic behavior is observed for the values of $D_{\pm}^{(k)}$ along the shadow curve, which is in distinct contrast to the results obtained within MSA.

Finally, and similar to the MSA, the curves of the average (positive or negative) charge of the particles as functions

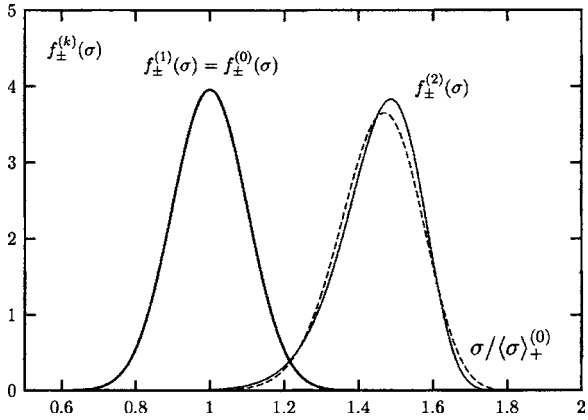


FIG. 5. As Fig. 4 for points $B_1$ and $B_2$ located on the cloud and shadow curves of system I (see Table I and Fig. 2).

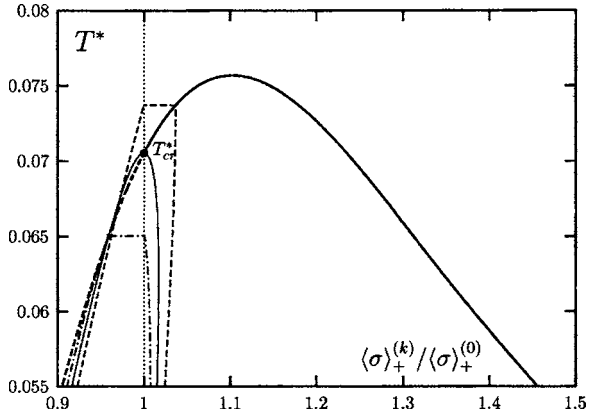


FIG. 6. $\langle\sigma\rangle_{+}^{(k)}[=\langle\sigma\rangle_{-}^{(k)}]$, $k=1,2$, as defined in the text (cf. Sec. IV A) for the size-symmetric polydisperse CHS mixture (system I) along three binodals for the parent phase densities $\rho^{*(0)}=0.04$ (broken line), $\rho^{*(0)}=\rho_{\text{cr}}^{*}=0.0641$ (full line), and $\rho^{*(0)}=0.1$ (dashed-dotted line), and along the shadow curve (thick full and thick broken lines). The dotted vertical line through $\langle\sigma\rangle_{+}^{(k)}/\sigma_{+}^{(0)}=1$ separates the gas (left) from the fluid (right) region. Note that this vertical line represents the $\langle\sigma\rangle_{+}^{(k)}/\sigma_{+}^{(0)}$ values for states on the cloud curve.

of the temperature show a similar behavior as the one observed for the $\langle\sigma\rangle_{\pm}^{(k)}$, which is certainly due to the assumed relation between charge and size of the particles, i.e., Eq. (14); we have not displayed these results.

### 3. Results for system II

The size-asymmetric case of a polydisperse mixture of CHS, i.e., system II, has a richer phase behavior and is thus more interesting. We start again with the PMSA phase diagram in Fig. 8, showing the cloud and shadow curves, along with three binodals for three selected densities, i.e., $\rho^{*}=0.04$, 0.2, and 0.102 (critical binodal). For reference we have added the binodal curve for the size-symmetric (bidisperse) primitive model for electrolytes, treated within the PMSA. In Fig. 9 we show the phase diagram of system II, comparing now PMSA with MSA. Again, the daughter dis-

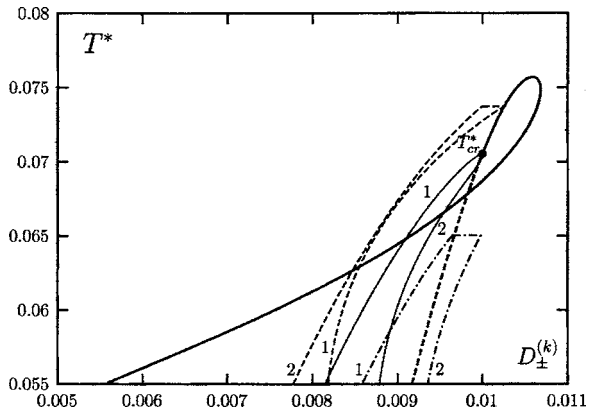


FIG. 7. $D_{+}^{(k)}[=D_{-}^{(k)}]$, $k=1,2$, as defined in the text (cf. Sec. IV A) for the size-symmetric polydisperse CHS mixture (system I) along three binodals for the parent phase densities $\rho^{*(0)}=0.04$ (broken line), $\rho^{*(0)}=\rho_{\text{cr}}^{*}=0.0641$ (full line), and $\rho^{*(0)}=0.1$ (dashed-dotted line), and along the shadow curve (thick full and thick broken lines). Binodals: $k=1$—gas phase, $k=2$—fluid phase; shadow curve: broken line—gas phase, full line—fluid phase.

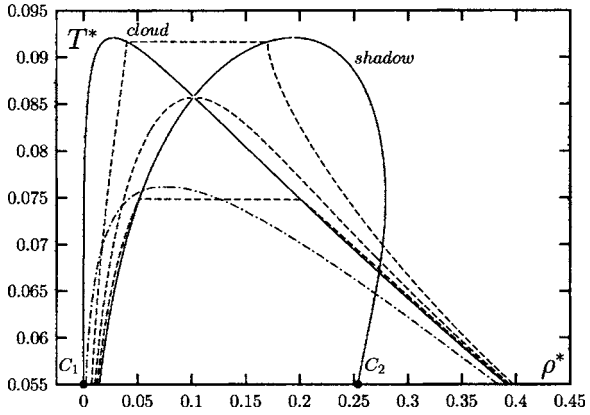


FIG. 8. Phase diagram ($T^*$ vs $\rho^*$) of the size-asymmetric polydisperse CHS mixture (system II) specified in the text. Cloud and shadow curves are represented by the solid lines (as labeled), binodals by the broken lines: the values of the densities of the respective parent phase $\rho^{*(0)}$ can be identified from the intersection of the binodal with the cloud curve: $\rho^{*(0)}=0.04$, 0.2, and 0.102 (critical binodal). A pair of points $(C_k, k=1,2)$ has been chosen on the cloud and shadow curves which is specified in Table I. The dash-dotted line denotes the binodal curve for a size-asymmetric (bidisperse) primitive model for electrolytes [with a diameter ratio of $\sigma_-^{(0)}/\sigma_+^{(0)}=0.7$] treated within the PMSA (Ref. 19).

tribution functions for one selected pair of points (located on the cloud and shadow curves) will be displayed in the following.

We observe a distinct influence on the shift of the critical point (both with respect to temperature and to density) as we compare the data of the bidisperse and the polydisperse model on the level of the PMSA. However, with respect to the size-symmetric case (system I), the shift is now less pronounced in temperature and in density. Compared to the MSA, the shift is similar as in the size-symmetric case (cf. Fig. 1) and again a strong asymmetry is introduced, in particular, in the shadow curve; within PMSA the cloud curve is of similar symmetry as in the MSA, its maximum is shifted to larger $\rho$ and smaller $T$ values.

We have then studied fractionation effects, starting again with the daughter distribution functions $f_\pm^{(k)}(\sigma)$ for selected points. In most cases we have observed qualitatively similar results as in the MSA and we thus display only one example,

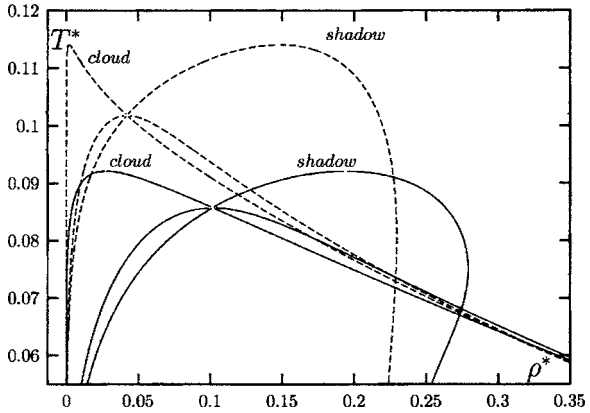


FIG. 9. Comparison of the phase diagram (in terms of cloud and shadow curves and the critical binodals) for the size-asymmetric polydisperse CHS mixture (system II) calculated via MSA (Ref. 5) (dashed lines) and PMSA (solid lines).

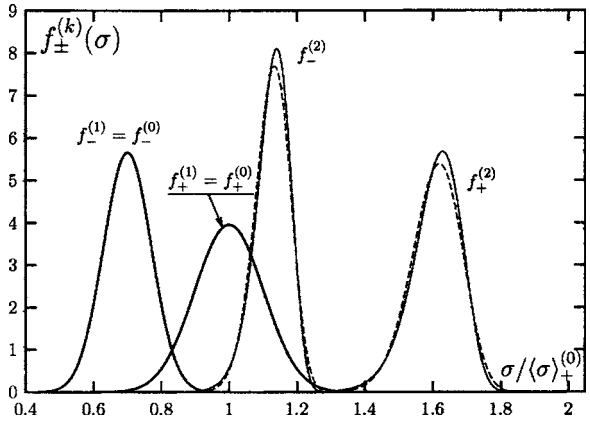


FIG. 10. Parent $[f_\pm^{(0)}(\sigma)]$ (thick full lines) and daughter $[f_\pm^{(k)}(\sigma), k=1,2]$ distribution functions (full lines) for the size-asymmetric polydisperse CHS mixture (system II) calculated for points $C_1$ and $C_2$, located on the cloud and shadow curves in the phase diagram (see Table I and Fig. 9). Broken lines: $f_\pm^{(k);\mathrm{beta}}(\sigma)$ as defined in the text. $k=1$—gas phase, $k=2$—fluid phase.

where we have found particular differences. It is a pair of state points (labeled $C_k$, $k=1,2$) which is located on the cloud and shadow curves (as indicated in Fig. 8 and specified in Table I). The corresponding $f_\pm^{(k)}(\sigma)$ are displayed in Fig. 10. For both positively and negatively charged particles we observe a clear separation of the daughter distribution functions of the coexisting phases, i.e., there is no overlap between the respective sets of curves, which offers a nice possibility to separate the larger particles in the liquid and the smaller particles in the gas phase.

To obtain a more quantitative information about fractionation effects we discuss the results for $\langle\sigma\rangle_\pm^{(k)}$, $D(k)_\pm$, and $\langle z_\pm\rangle_\pm^{(k)}$. As a consequence of the local charge neutrality requirement (11) in the present model the situation is different than in the MSA case: we reconsider Eq. (20) and multiply both sides with $\sigma$; integration leads to

$$\langle\sigma\rangle_-^{(k)} = \langle\sigma\rangle_+^{(k)} K, \quad k=0,1,2, \tag{78}$$

$K$ being defined in (77). Therefore $\langle\sigma\rangle_+^{(k)}/\langle\sigma\rangle_+^{(0)} = \langle\sigma\rangle_-^{(k)}/\langle\sigma\rangle_-^{(0)}$, $k=1,2$. In a similar manner one can easily derive

$$\langle\sigma\rangle_- = \langle\sigma\rangle_+ K^2 \tag{79}$$

and thus $D_-^{(k)}=D_+^{(k)}$, $k=1,2$. This means that only results for the positively or negatively charged particles need to be discussed.

The curves for $\langle\sigma\rangle_+^{(k)}/\langle\sigma\rangle_+^{(0)}$ (cf. Fig. 11) show similar shapes as in the MSA.[5] Here a brief comment on the corresponding MSA curves (shown in Figs. 11 and 12 of Ref. 5) is in order: from these data one might conclude that MSA leads to considerable differences between the + and the − case. However, if these figures are redrawn with the same scaling of the diameters as in the present contribution, then the + and the − curves are considerably closer and they sometimes even coincide; only for the high-density branch of the shadow curve considerable differences are only encountered. While the local charge neutrality of the present concept imposes the scaling behavior (78), this behavior is automatically satisfied within a remarkably high accuracy for MSA.

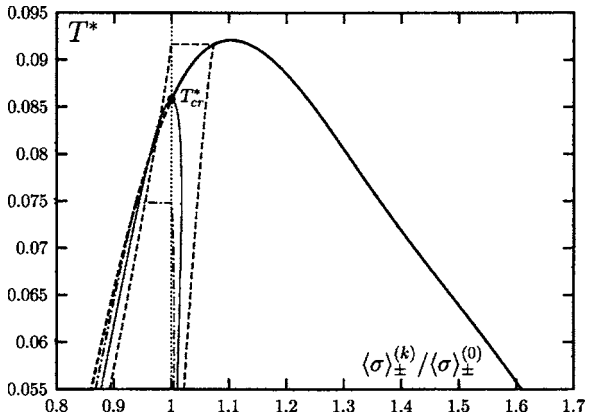


FIG. 11. $\langle\sigma\rangle^{(k)}_{+}/\langle\sigma\rangle^{(0)}_{+}=(\langle\sigma\rangle^{(k)}_{-}/\langle\sigma\rangle^{(0)}_{-})$, $k=1,2$, as defined in the text (cf. Sec. IV A) for the size-asymmetric polydisperse CHS mixture (system II) along three binodals for the parent phase densities $\rho^{*(0)}=0.04$ (broken line), $\rho^{*(0)}=\rho^{*}_{\mathrm{cr}}=0.102$ (full line), and $\rho^{*(0)}=0.2$ (dashed-dotted line), and along the shadow curve (thick full and thick broken lines). The dotted vertical line through $\langle\sigma\rangle^{(k)}_{\pm}/\sigma^{(0)}_{+}=1$ separates the gas (left) from the fluid (right) region. Note that this vertical line represents the $\langle\sigma\rangle^{(k)}_{\pm}/\langle\sigma\rangle^{(0)}_{\pm}$ values for states on the cloud curve.

We therefore conclude that the local charge neutrality condition does not really represent a considerable restriction. Finally, we observe that $D^{(k)}_{\pm}$ behaves in a similar manner as in the size-symmetric model (cf. Fig. 12) and therefore shows distinct difference with respect to the MSA. Finally, the average charges, $\langle z_{\pm}\rangle^{(k)}_{\pm}$, $k=1,2$, show—as a consequence of relation (14)—a similar behavior as $\langle\sigma_{\pm}\rangle^{(k)}_{\pm}$, and therefore do not display them here.

### D. Outlook

The deplorable lack of computer simulation reference data for the location of the critical point in polydisperse mixtures of CHS has motivated us to an admittedly speculative study how $T_{\mathrm{cr}}$ and $\rho_{\mathrm{cr}}$ might vary with size asymmetry [at fixed distribution width $D^{(0)}=0.01$.]

In Fig. 13 we show the values for the critical temperature and the critical density as obtained in the MSA and in the PMSA as functions of the size-asymmetry parameter $\tau=\langle\sigma\rangle^{(0)}_{-}/\langle\sigma\rangle^{(0)}_{+}$, keeping $D^{(0)}$ fixed to 0.01. Similar as in the case of the bidisperse CHS mixture (see Fig. 1), the PMSA data are shifted with respect to the MSA results to lower values in $T_{\mathrm{cr}}$ and to higher values in $\rho_{\mathrm{cr}}$: as we have learned from the bidisperse case (see Sec. IV C 1), this represents a shift just in a direction where discrepancies with (exact) computer simulation data become smaller. In an effort to *estimate* the location of the exact data, we *assume* that the MSA, the PMSA, and the exact values for the critical parameters satisfy, regardless of the degree of polydispersity, the following relations:

$$\frac{T^{*}_{\mathrm{cr;MSA}}-T^{*}_{\mathrm{cr;PMSA}}}{T^{*}_{\mathrm{cr;PMSA}}-T^{*}_{\mathrm{cr;MC}}}=C_1,\quad \frac{\rho^{*}_{\mathrm{cr;MSA}}-\rho^{*}_{\mathrm{cr;PMSA}}}{\rho^{*}_{\mathrm{cr;PMSA}}-\rho^{*}_{\mathrm{cr;MC}}}=C_2. \quad (80)$$

Inserting our results and the results of MC simulation studies[12,13] for bidisperse size-asymmetric primitive electrolyte model in the above relations, the two constants $C_1$ and $C_2$ in relation (80) can be fixed. Extending now this extrapolation expression to *all* $\tau$ values, we obtain the dotted curve shown in Fig. 13.

In a similar manner we study the influence of polydispersity on the location of the critical point; we restrict ourselves here to the size-symmetric case. Using an extrapolation procedure as the one outlined above, we obtain $T_{\mathrm{cr}}$ and $\rho_{\mathrm{cr}}$ as functions of $D^{(0)}$ (Fig. 14). Based on this extrapolation we expect $T_{\mathrm{cr}}$ to increase with increasing polydispersity

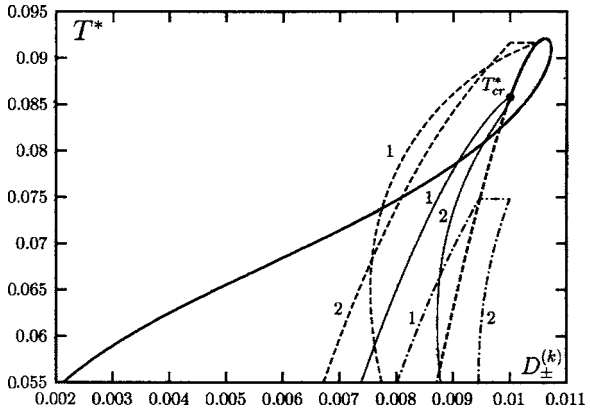


FIG. 12. $D^{(k)}_{+}(=D^{(k)}_{-})$, $k=1,2$, as defined in the text (cf. Sec. IV A) for the size asymmetric polydisperse CHS mixture (system II) along three binodals for the parent phase densities $\rho^{*(0)}=0.04$ (broken line), $\rho^{*(0)}=\rho^{*}_{\mathrm{cr}}=0.102$ (full line), and $\rho^{*(0)}=0.2$ (dashed-dotted line), and along the shadow curve (thick full and thick broken lines). Binodals: $k=1$—gas phase, $k=2$—fluid phase; shadow curve: broken line—gas phase, full line—fluid phase.

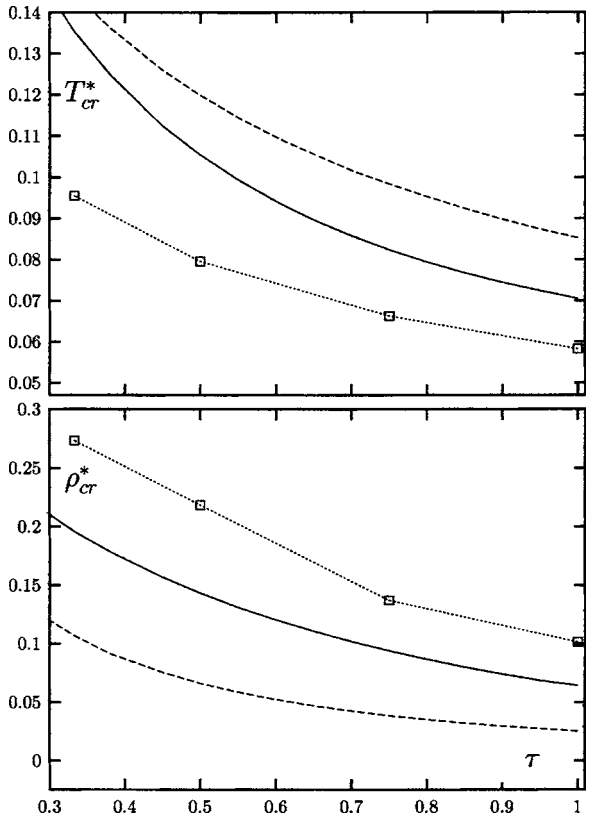


FIG. 13. Critical temperature $T^{*}_{\mathrm{cr}}$ (top) and critical density $\rho^{*}_{\mathrm{cr}}$ (bottom) vs $\tau=\langle\sigma\rangle^{(0)}_{-}/\langle\sigma\rangle^{(0)}_{+}$ at fixed polydispersity $D^{(0)}=0.01$ for the polydisperse CHS fluid, as predicted using MSA (Ref. 5) (dashed lines) PMSA (solid lines) data and the extrapolation scheme presented in Sec. IV D: open squares; the dotted lines connecting symbols are shown to guide the eye.

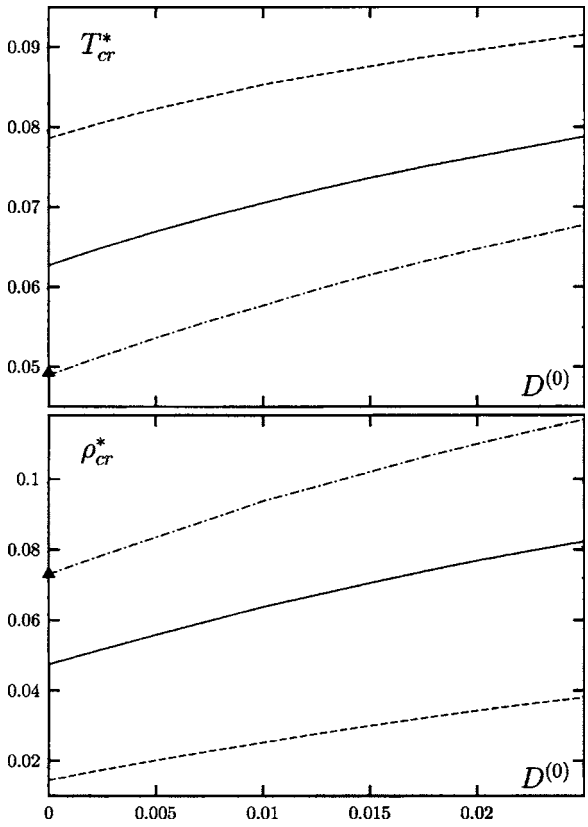


FIG. 14. Critical temperature $T^*_{cr}$ (top) and critical density $\rho^*_{cr}$ (bottom) vs $D^{(0)}$ for a polydisperse mixture of CHS (as described in Sec. IV D): MSA (Ref. 5) (dashed lines), PMSA (solid lines); MC (Refs. 44–46) data (filled triangles) for the RPM [i.e., $D^{(0)}=0$] are given for reference. For the dash-dotted line see text.

which is plausible, since the increasing number of larger particles will induce a stronger interaction among the particles.

## V. CONCLUSIONS

In an effort to study the phase behavior of a polydisperse mixture of CHS on a more quantitative level than this is possible within the framework of the MSA, we have generalized the concept of MSNC to the polydisperse case. The resulting polydisperse mixture of neutral, polar dimers is then treated within the PMSA. Generalizing the expressions for the thermodynamic properties from the case of a mixture with a finite number of components to the polydisperse case we realize that they can be expressed by a finite number of generalized moments of the distribution function that characterizes the polydispersity of the system. Thus, instead of solving the infinitely many coexistence equations we can determine the densities and the distribution functions of the coexisting daughter phases by solving a set of coupled, nonlinear equations. We have chosen two polydisperse mixtures of CHS, one being size symmetric, the other one being asymmetric in size with $\tau=0.7$. Due to the lack of simulation results for the critical parameters of these systems we can only estimate that PMSA is indeed able to shift—similar to the bidisperse case—the location of the critical point in such a direction that the discrepancy becomes smaller.

In an effort to reduce these differences we plan the following modifications of the concept: reflecting observations of simulations[14] that up to 40%–50% neutral dimers and up to 20%–30% neutral tetramers are counted in the RPM close to phase boundaries, we also intend to include these higher-order clusters in the concept. This will certainly lead to a considerably increased complexity of the formalism and, as a consequence, to numerical problems; however, we expect that inclusion of these effects will shift the PMSA curves even closer to "exact" simulation data.

## ACKNOWLEDGMENTS

This work was supported by the Österreichischer Forschungsfonds (FWF) under Project Nos. P14371, P15785, and P17823 and by the Österreichisches Bundesministerium für Bildung, Wissenschaft und Kultur under Project No. GZ 45.492/1-VI/B/7a/2002. One of the authors (Y.V.K.) gratefully acknowledges the hospitality at the CMS and the Institut für Theoretische Physik at the TU Wien where part of this work was performed.

[1] H. Weingärtner and W. Schröer, Adv. Chem. Phys. **116**, 1 (2001).
[2] J.-P. Hansen and I. R. McDonald, *Theory of Simple Liquids*, 2nd ed. (Academic, New York, 1986).
[3] N. B. Wilding, M. Fasolo, and P. Sollich, J. Chem. Phys. **121**, 6887 (2004).
[4] P. Sollich, J. Phys.: Condens. Matter **14**, R79 (2002).
[5] Yu. V. Kalyuzhnyi, G. Kahl, and P. T. Cummings, J. Chem. Phys. **120**, 10133 (2004).
[6] J. J. Salacuse and G. Stell, J. Chem. Phys. **77**, 3714 (1982).
[7] L. Blum, Mol. Phys. **30**, 1529 (1975).
[8] L. Blum and J. S. Høye, J. Phys. Chem. **81**, 1311 (1977).
[9] J.-M. Caillol and J.-J. Weis, J. Chem. Phys. **102**, 7610 (1995).
[10] F. Bresme, E. Lomba, J.-J. Weis, and J. L. F. Abascal, Phys. Rev. E **51**, 289 (1995).
[11] J. C. Shelley and G. N. Patey, J. Chem. Phys. **103**, 8299 (1995).
[12] J. M. Romero-Enrique, G. Orkoulas, A. Z. Panagiotopoulos, and M. E. Fisher, Phys. Rev. Lett. **85**, 4558 (2000).
[13] Q. Yan and J. J. de Pablo, J. Chem. Phys. **114**, 1727 (2001).
[14] J. M. Romero-Enrique, L. F. Rull, and A. Z. Panagiotopoulos, Phys. Rev. E **66**, 041204 (2002).
[15] D. W. Cheong and A. Z. Panagiotopoulos, J. Chem. Phys. **119**, 8526 (2003).
[16] M. J. Gillan, Mol. Phys. **49**, 421 (1983).
[17] G. Stell, J. Stat. Phys. **78**, 197 (1995).
[18] B. Guillot and Y. Guissani, Mol. Phys. **87**, 37 (1996).
[19] Yu. V. Kalyuzhnyi, Mol. Phys. **94**, 735 (1998).
[20] Yu. V. Kalyuzhnyi, M. F. Holovko, and V. Vlachy, J. Stat. Phys. **100**, 243 (2000).
[21] Yu. V. Kalyuzhnyi and P. T. Cummings, J. Chem. Phys. **115**, 540 (2001); **116**, 8637 (2002).
[22] J. W. Jiang, L. Blum, and O. Bernard, Mol. Phys. **99**, 1765 (2001).
[23] J. W. Jiang, L. Blum, O. Bernard, J. M. Prausnitz, and S. I. Sandler, J. Chem. Phys. **116**, 7977 (2002).
[24] M. F. Holovko and Yu. V. Kalyuzhnyi, Mol. Phys. **73**, 1145 (1991).
[25] Yu. V. Kalyuzhnyi, Mol. Phys. **94**, 735 (1998).
[26] Yu. V. Kalyuzhnyi and G. Stell, Chem. Phys. Lett. **240**, 157 (1995).
[27] Yu. V. Kalyuzhnyi and P. T. Cummings, J. Chem. Phys. **103**, 3265 (1995).
[28] Yu. V. Kalyuzhnyi, C.-T. Lin, and G. Stell, J. Chem. Phys. **106**, 1940 (1997).
[29] C.-T. Lin, Yu. V. Kalyuzhnyi, and G. Stell, J. Chem. Phys. **108**, 6513 (1998).
[30] Yu. V. Kalyuzhnyi, C.-T. Lin, and G. Stell, J. Chem. Phys. **108**, 6525 (1998).
[31] M. S. Wertheim, J. Stat. Phys. **35**, 19 (1984); **35**, 35 (1984).
[32] M. S. Wertheim, J. Stat. Phys. **42**, 495 (1986); **42**, 477 (1986).
[33] Yu. V. Kalyuzhnyi, G. Kahl, and P. T. Cummings, Europhys. Lett. **72** (2005) (in press).
[34] O. Bernard and L. Blum, J. Chem. Phys. **104**, 4746 (1996).
[35] O. Bernard and L. Blum, J. Chem. Phys. **112**, 7227 (2000).

[36] M. S. Wertheim, J. Chem. Phys. **85**, 2929 (1986).
[37] G. A. Mansoori, N. F. Carnahan, K. E. Starling, and T. W. Leland, J. Chem. Phys. **54**, 1523 (1971).
[38] Yu. V. Kalyuzhnyi and G. Kahl, J. Chem. Phys. **119**, 7335 (2003); **112**, 1168 (2004).
[39] L. Bellier-Castella, H. Xu, and M. Baus, J. Chem. Phys. **113**, 8337 (2000).
[40] L. Bellier-Castella, M. Baus, and H. Xu, J. Chem. Phys. **115**, 3381 (2001).
[41] J. A. Gualtieri, J. M. Kincaid, and G. Morrison, J. Chem. Phys. **77**, 52 (1982).
[42] Note that the first factor on the right-hand side of the following equation had erroneously been omitted in Eq. (34) of Ref. 38 and in Eq. (66) of Ref. 5.
[43] M. Abramowitz and I. A. Stegan, *Handbook of Mathematical Functions*, Applied Mathematical Series Vol. 55 (National Bureau of Standards, Washington, D.C., 1964).
[44] J.-M. Caillol, D. Levesque, and J.-J. Weis, J. Chem. Phys. **107**, 1565 (1997).
[45] G. Orkoulas and A. Z. Panagiotopoulos, J. Chem. Phys. **110**, 1581 (1999).
[46] Q. Yan and J. J. de Pablo, J. Chem. Phys. **111**, 9509 (1999).